JOURNAL OF Materials CHEMISTRY

Magnetic properties of γ-Fe_2O_3–SiO_2 aerogel and xerogel nanocomposite materials

Carla Cannas,[a] Maria F. Casula,[a] Giorgio Concas,[b] Anna Corrias,*[a] Dante Gatteschi,[c] Andrea Falqui,[b] Anna Musinu,[a] Claudio Sangregorio[c] and Giorgio Spano[b]

[a]*Dipartimento di Scienze Chimiche, Università di Cagliari, S.P. Monserrato-Sestu Km 0.700, I-09042 Monserrato (Cagliari), Italy. Tel: +39 070 6754351; Fax: +39 070 6754388; E-mail: corrias@unica.it*
[b]*Dipartimento di Fisica, Università di Cagliari, and Istituto Nazionale per la Fisica della Materia, S.P. Monserrato-Sestu Km 0.700, I-09042 Monserrato (Cagliari), Italy*
[c]*Dipartimento di Chimica, Università di Firenze, Via Maragliano 75, I-50144 Firenze, Italy*

Received 23rd May 2001, Accepted 14th August 2001
First published as an Advance Article on the web 9th October 2001

The properties of aerogel and xerogel iron oxide–silica nanocomposites prepared by the sol–gel method were investigated by thermal analysis, X-ray diffraction, transmission electron microscopy, Mössbauer spectroscopy and susceptibility measurements. Pure maghemite nanoparticles were obtained starting from both xerogel and aerogel samples, with particles of average size around 5 nm which tend to aggregate into the silica matrix. The role of magnetic interparticle interactions, which have a strong influence on the magnetic properties, is discussed.

Introduction

In recent years there has been a great deal of interest in nanocomposites containing maghemite nanoparticles dispersed in polymeric, glassy or ceramic matrices.[1–3] Maghemite (γ-Fe_2O_3) in itself is a material of great technological importance for its use in magnetic recording systems and in catalysis; moreover, maghemite properties are particularly enhanced when the size of the particles reaches the nanometer range.[4–7] Although nanosized γ-Fe_2O_3 transforms into α-Fe_2O_3 (hematite) at rather low temperatures ($\sim$350 °C)[1,8] it can be stabilized through the incorporation of the nanoparticles into polymeric, glassy or ceramic matrices.[1–3]

Among the various preparation procedures which can be used to obtain Fe_2O_3–SiO_2 nanocomposites the sol–gel method has been proven to offer some interesting features which allow control of the final properties of the materials.[9] In particular the porous structure of the matrix can be tailored by properly choosing the experimental conditions. In particular, when the solvent is removed from the alcogel by usual heating, the capillary forces at the liquid/vapor interface produce shrinkage and cracking so that the original porous structure is lost and dense xerogels are obtained. On the other hand, when the solvent is removed above its critical parameters, T_c and P_c, aerogels with high surface areas and pore volumes are obtained since the skeletal alcogel structure can be preserved.[10]

In previous investigations we have shown that the stabilization of maghemite can be achieved in xerogel samples up to a certain iron content[11] while it seems that the stabilization is much more difficult in the aerogel samples.[12] However, the stabilization of maghemite seems to depend strongly on the alcogel preparation conditions since other authors have shown that the maghemite phase can be stabilized in xerogel samples in a wide concentration range by using a slightly different sol–gel procedure.[13]

Since the porous structure can have a great influence on the stabilization of the maghemite nanoparticles in the silica matrix it is of interest to compare the results on xerogel and aerogel nanocomposites prepared using the same sol–gel procedure. In particular, in this paper we present a detailed study of the magnetic properties of maghemite–silica xerogel and aerogel nanocomposites synthesized by a sol–gel method similar to that reported in ref. 13 and characterized by thermal analysis (TG, DTA), X-ray diffraction (XRD), transmission electron microscopy (TEM) and Mössbauer spectroscopy. The superparamagnetic relaxation was investigated by both magnetic susceptibility measurements and Mössbauer spectroscopy. The coercive field and the reduced remanent magnetization were obtained through hysteresis curves at low temperature (3 K). Information on the dynamics of the reversal of the magnetization was obtained through a.c. susceptibility measurements.

Experimental procedure

Iron oxide–silica gels were prepared using iron nitrate nonahydrate (Aldrich, 98%) and tetraethoxysilane (TEOS, Aldrich, 98%) as metal oxide and silica precursors respectively and ethanol (Carlo Erba, 99%) as mutual solvent, following a similar procedure to that reported in ref. 13. The nominal composition of the final nanocomposite is 25% wt. of iron oxide ($Fe_2O_3/(Fe_2O_3+SiO_2)$). The sol, which had an initial pH of about 1, was poured into four vessels with an initial surface/volume ratio of about 0.02. The vessels, closed using a seal into which a small hole was punched, were put in an oven at 50 °C: under these conditions gelation occurs within about 11 days. The gelation times of the four batches were slightly different probably due to differing sizes of the holes.

Two xerogel samples were obtained by thermally treating two fresh monolithic gels, which had slightly different gelation times, in a preheated oven in static air at 400 °C for 4 hours (the samples will be hereafter denoted X_1-T4 and X_2-T4). Two aerogel samples (samples A_1 and A_2) were obtained by high temperature supercritical drying of two fresh monolithic gels, with slightly different gelation times, in an autoclave (Parr, 300 cm^3) partially filled with absolute ethanol. The autoclave, initially pressurized with nitrogen up to 7 atm, was heated up to 200 °C at 1 °C min^{-1} and then to 300 °C at 0.5 °C min^{-1}. The monolithic aerogels as extracted were then submitted to the same thermal treatment as the xerogel samples, *i.e.* in a preheated oven in static air at 400 °C for 4 hours (samples

 DOI: 10.1039/b104562h

A_1-T4 and A_2-T4). The same thermal treatment at 400 °C for 4 hours was also performed on the aerogel samples after finely grinding them in an agate mortar (samples A_1P-T4, A_2P-T4).

Thermogravimetry (TG) and simultaneous differential thermal analysis (DTA) of the fresh gels and of the aerogels were carried out on a Mettler-Toledo TGA/STDA 851. Thermal analysis data were collected in the range 25–1000 °C, under oxygen flow (heating rate = 10 °C min^{-1}; flow rate = 50 cm^3 min^{-1}).

XRD spectra were recorded on a D500 Siemens diffractometer equipped with a graphite monochromator on the diffracted beam. The scans were collected in the range from 4 to 44° (2θ) using MoKα radiation.

TEM micrographs were recorded on a JEOL 200CX microscope operating at 200 kV. The finely powdered samples were dispersed in n-octane and dropped on a conventional carbon-coated copper grid.

Mössbauer absorption spectra were obtained in standard transmission geometry, using a source of ^{57}Co in rhodium (370 MBq). Calibration was performed using a 25 μm thick natural iron foil; the isomer shift values are referenced to α-Fe. The measurements at room temperature were carried out on powdered samples kept in a plexiglas holder. The surface density of the absorbers ranges from 50 to 80 mg cm^{-2}.

The measurements at low temperature were carried out using a flow cryostat with mylar windows; nitrogen was used as the cryogenic liquid. These measurements were performed using a copper sample holder placed in the exchange gas; the powders were kept between two layers of Plexiglass. The surface density of the absorbers ranges from 50 to 80 mg cm^{-2}.

The absorption spectra were adequately simulated by peaks with Lorentzian shape, which is the basic shape in the resonant absorption of γ photons. The spectra at room temperature of the X_1-T4 and A_1-T4 samples were fitted by a single quadrupole doublet with free parameters, using a least squares method. In superparamagnetic materials near the blocking temperature, this fitting procedure is an approximation because superparamagnetic materials do not show simple Lorentzian line shapes, owing to the presence of phenomena of paramagnetic relaxation.[14] In samples with only one size of nanoparticles, the line shape suggested by Wickman[14] can be used while in samples with a distribution of particle sizes, the usual procedure is the use of a Lorentzian sextet for the blocked particles and a Lorentzian doublet for the non-blocked particles.[15,16] Therefore we followed this last procedure in the fit of the spectra at low temperature, which show blocked and non-blocked magnetic states.

Static magnetizations and a.c. magnetic susceptibilities were measured using a S600 Cryogenic Squid magnetometer. Zero-field-cooled (ZFC) magnetization curves were obtained by cooling samples to the lowest measuring temperature in zero magnetic field and then by measuring the magnetization at stepwise increasing temperatures with an applied field of 50 Oe. Field-cooled (FC) curves were recorded after cooling the samples in the measuring field of 50 Oe.

A.c. susceptibility measurements were performed at different frequencies in the range 0.18–510 Hz with an exciting amplitude of 1 V corresponding to an oscillating field of 0.1 Oe.

Results and discussion

Thermal analysis

The TG curves for the four fresh gels, which are reported in Fig. 1(A), show a remarkable mass loss in the low temperature range which is due to solvent removal and decomposition of iron nitrate, while the mass loss is very limited for temperatures higher than 300 °C. The four fresh gels present some differences in the total mass loss, as a consequence of the slightly different gelation times; in particular, the samples with the higher mass loss are the ones which gel first. This result indicates that the samples with shorter gelation times contain a larger amount of solvent entrapped in the pores. The X_1 xerogel sample was prepared starting from the gel which presents the largest mass loss, and the A_1 aerogel sample was obtained from the gel with the smallest mass loss.

In Fig. 1(B) the corresponding DTA curves are shown; in agreement with the TG results, some differences among the four curves are detectable in the low temperature range where endothermic peaks are present due to solvent removal and decomposition of iron nitrate. Broad exothermic peaks due to the combustion of organic residues are present around 300 °C.

The TG curves and the corresponding DTA curves for the A_1 and A_2 aerogel samples are reported in Fig. 2(A) and (B). The mass loss at low temperature is now very limited as a consequence of supercritical solvent extraction and no endothermic peak is present in the DTA curves. An appreciable mass loss is detectable between 250 and 500 °C which corresponds to strong exothermic peaks in the DTA curves. This is due to the combustion of organics which mainly arise from the re-esterification of silanols by the ethanol present in the autoclave during supercritical extraction.[17] The DTA curves of the two aerogel samples are significantly different since the A_2 sample shows a single intense exothermic peak centered around 300 °C while the A_1 sample shows a double peak whose components are centered at 300 and 375 °C.

These results seem to indicate some differences in the location of the organic residues in the two aerogel samples. In fact, it has already been pointed out that DTA curves of aerogel nanocomposite materials can present exothermic peaks at somewhat different temperatures depending on how easily the organics can be reached by the oxygen gas.[18] It seems that the A_1 aerogel sample, which is obtained from a gel containing less solvent than the A_2 one, presents some organics which are either very superficial or not tightly bound and some others which are much more difficult to reach. In sample A_2 the organics are all burnt off in a smaller temperature range giving rise to a single intense exothermic peak.

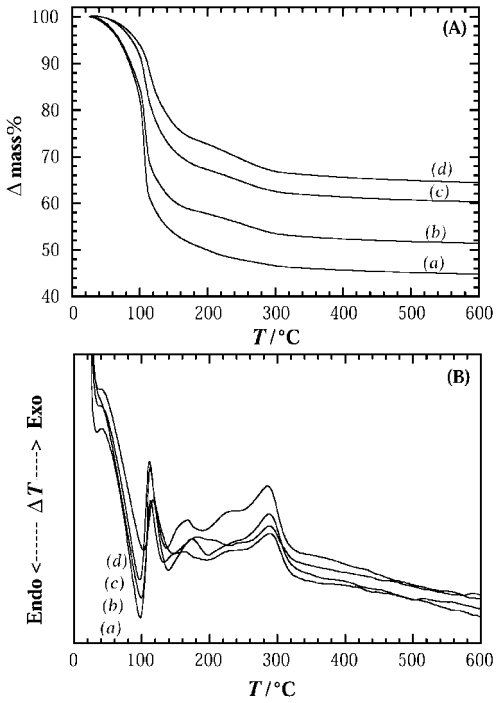

Fig. 1 TG (A) and DTA (B) curves for the four gels which were used to produce the X_1 (a), A_2 (b), X_2 (c) and A_1 (d) samples.

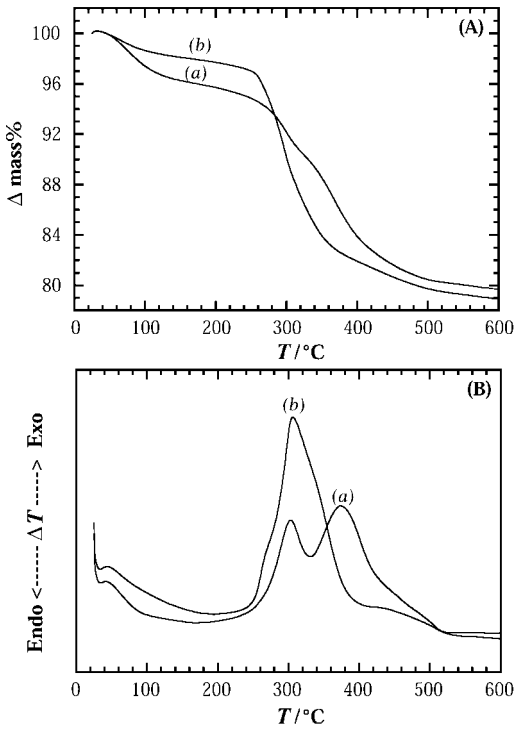

Fig. 2 TG (A) and DTA (B) curves for the A_1 (a) and A_2 (b) samples.

TEM and XRD

The TEM observations of the A_1 and A_2 aerogel samples before heat treatment and of the A_1-T4, A_2-T4, X_1-T4 and X_2-T4 samples evidence a very similar morphology, showing nanoparticles located in large and irregular aggregates (with dimensions ranging from 20 to 250 nm), or islands, within the amorphous matrix. Some examples of the TEM micrographs are reported in Fig. 3.

The crystallite size distribution is quite narrow. In particular, the particle size distributions which were derived from the dark field micrographs for the X_1-T4 and A_1-T4 samples (total number of particles *ca.* 1000) could be well reproduced by a log-normal size distribution with an average diameter $\langle D \rangle = 5.4 \pm 0.2$ nm and standard deviation $\sigma_D = 0.30$ for the X_1-T4 sample and $\langle D \rangle = 4.3 \pm 0.3$ nm and $\sigma_D = 0.43$ for the A_1-T4 sample.

Because of the small particle sizes no identification of the crystalline phase was possible from the microdiffraction patterns.

The XRD patterns of the A_1-T4, A_2-T4 , X_1-T4 and X_2-T4 samples are shown in Fig. 4. The spectra of both the xerogel samples and of the A_1-T4 sample exhibit broad peaks, superimposed on the amorphous silica halo, which can be attributed to the presence of nanocrystalline maghemite, γ-Fe_2O_3.[19] The line broadening indicates that the average crystallite size of the maghemite particles is a few nanometers in all the samples, in agreement with TEM results. However, some differences are detectable among the three samples. In particular, the main maghemite peak is slightly sharper in the X_1-T4 sample compared to the A_1-T4 and X_2-T4 samples; the latter is the one presenting the broadest peak. Finally, the spectrum of the A_2-T4 aerogel sample indicates the presence of a small amount of nanocrystalline hematite (α-Fe_2O_3) together with maghemite.[19]

The spectra of the A_1P-T4 and A_2P-T4 aerogel samples, treated at 400 °C after grinding, differ from the spectra of the

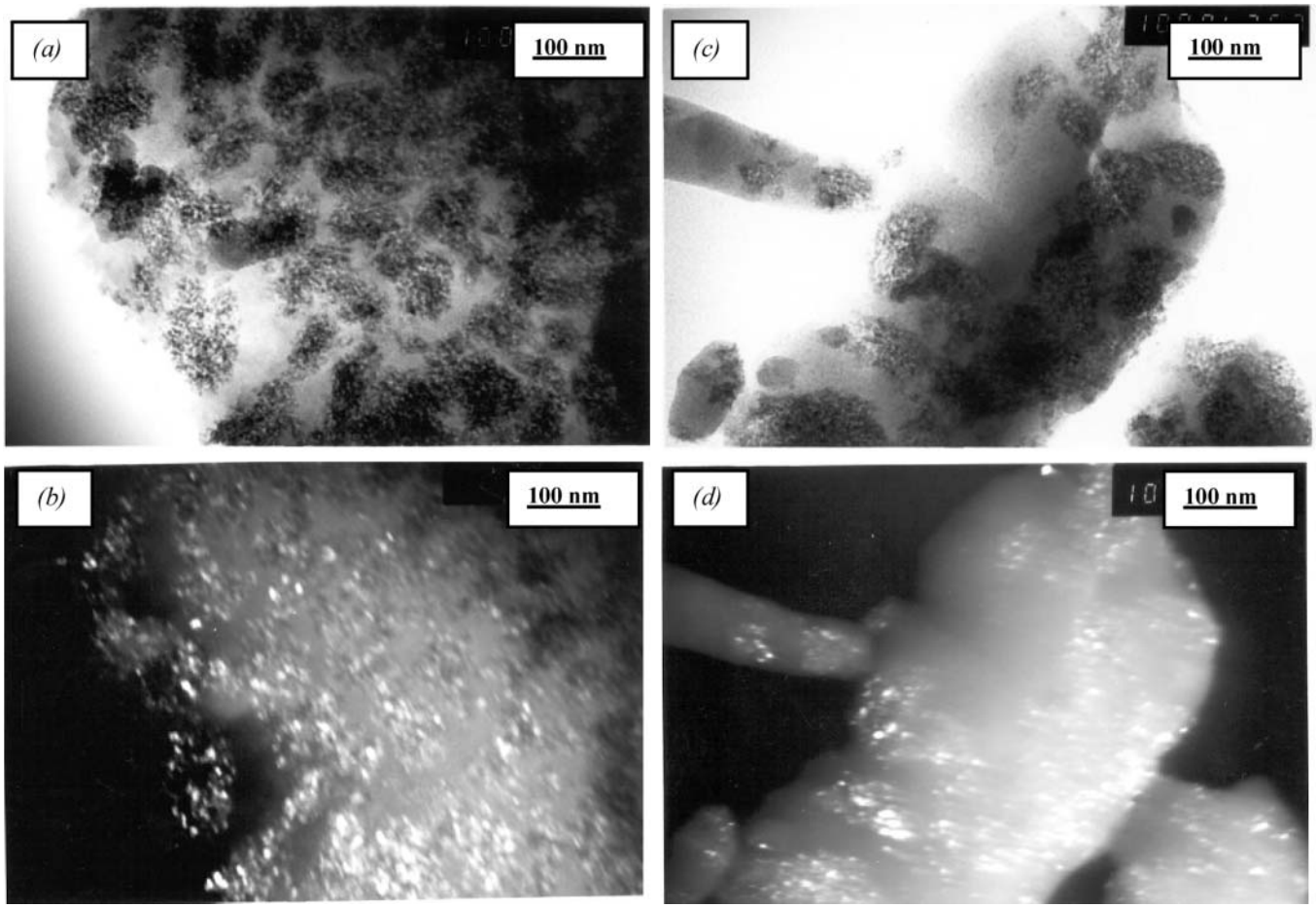

Fig. 3 TEM micrographs for X_1-T4 (left) and A_1-T4 (right) samples.

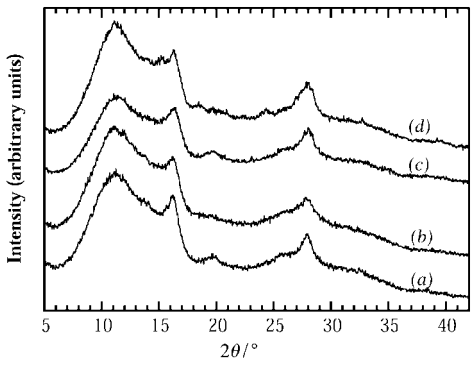

Fig. 4 XRD patterns for the (a) X_1-T4, (b) X_2-T4, (c) A_1-T4 and (d) A_2-T4 samples.

A_1-T4 and A_2-T4 samples in terms of the line broadening which is especially pronounced in the A_1P-T4 sample.

The XRD results indicate that the evolution of the samples with thermal treatment depends on the amount of solvent entrapped in the pores at the gelation point for both xerogel and aerogel samples, even if in a somewhat different way. In fact, the XRD spectra of X_1-T4 and X_2-T4 show that in both xerogel samples only maghemite nanoparticles are formed; the average particles size is, however, slightly larger in the X_1-T4 sample which was obtained from the gel containing a larger amount of solvent.

In the case of the aerogels, only the A_1 sample, obtained from the gel with the smallest amount of solvent, gives rise to the formation of a pure maghemite–silica nanocomposite, while the A_2-T4 sample shows the presence of some hematite together with maghemite.

It should be remarked that the DTA curve of the A_2 sample shows a single intense exothermic peak. It is likely that in this case the sample overheats during thermal treatment at 400 °C and the transition from γ- to α-Fe_2O_3 begins.

Mössbauer spectroscopy

In Fig. 5 the Mössbauer absorption spectra of the X_1-T4, A_1-T4 and A_2-T4 samples at 293 K are shown. In Table 1 the results of the least squares fitting are given; the values of isomer shift (δ), quadrupole splitting (Δ) and full width at half maximum (Γ) are reported.

The spectra of X_1-T4 and A_1-T4 show the features of superparamagnetic materials. All the spectra show components with values of isomer shift typical of trivalent iron;[20,21] the quadrupole splitting of the superparamagnetic component is consistent with this interpretation. These spectra can be fitted by a single doublet. The spectrum of the A_2-T4 sample also presents a Zeeman split component, this last contribution being due to the presence of a small amount of hematite. The impurity of hematite does not appear in the spectrum of the powdered aerogel sample A_2P-T4.

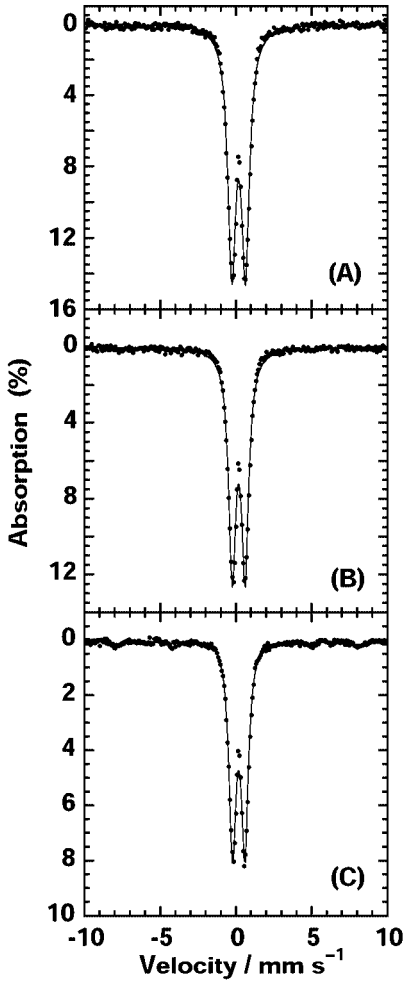

Fig. 5 Mössbauer spectra of the X_1-T4 (A), A_1-T4 (B) and A_2-T4 (C) samples at 293 K. The experimental points (dots) and the calculated data (solid line) are shown.

Fig. 6 shows the spectra of the X_1-T4 sample at 84 K and 77 K. At these temperatures the superparamagnetic component and the blocked component are both present. We used the simple Lorentzian approximation by fitting the spectra by one doublet and one sextet, which is the usual procedure used in similar materials.[15,16] The area of each component is proportional to the number of iron atoms belonging to nanoparticles in the non-blocked or blocked state and to the recoil-free

Table 1 Mössbauer parameters as obtained by fitting the spectra of the samples: the temperatures at which the spectra were collected and the values of the isomer shift (δ), the quadrupole splitting (Δ), the full width at half maximum of the peaks (Γ), the magnetic field (B), the area (A) of each component and the reduced chi-squared value (χ^2) are reported. Statistical errors are given in parentheses as errors on the last digit

Sample	T/K	δ/mm s^{-1}	Δ/mm s^{-1}	Γ/mm s^{-1}	B/T	A (%)	χ^2
X1-T4	293	0.34(1)	0.89(1)	0.63(1)			4.5
	84	0.45(1)	1.07(1)	0.81(1)		44(2)	2.3
		0.43(3)		2.9(1)	44.0(4)	56(6)	
	77	0.45(1)	1.08(1)	0.78(1)		33(1)	2.3
		0.41(2)		2.32(5)	44.4(2)	67(4)	
A1-T4	293	0.34(1)	0.84(1)	0.56(1)			4.1
	90	0.45(1)	0.96(1)	0.88(2)		44(3)	1.1
		0.47(4)		3.0(2)	39(1)	56(8)	
	77	0.44(1)	1.03(2)	0.92(4)		15(6)	1.7
		0.49(2)		2.68(5)	41.3(2)	85(4)	
A2-T4	293	0.34(1)	0.80(1)	0.55(1)		97(4)	3.7
		0.28(3)		1.0(1)	49.5(3)	3(1)	
A2P-T4	293	0.35(1)	0.81(1)	0.58(1)			1.9

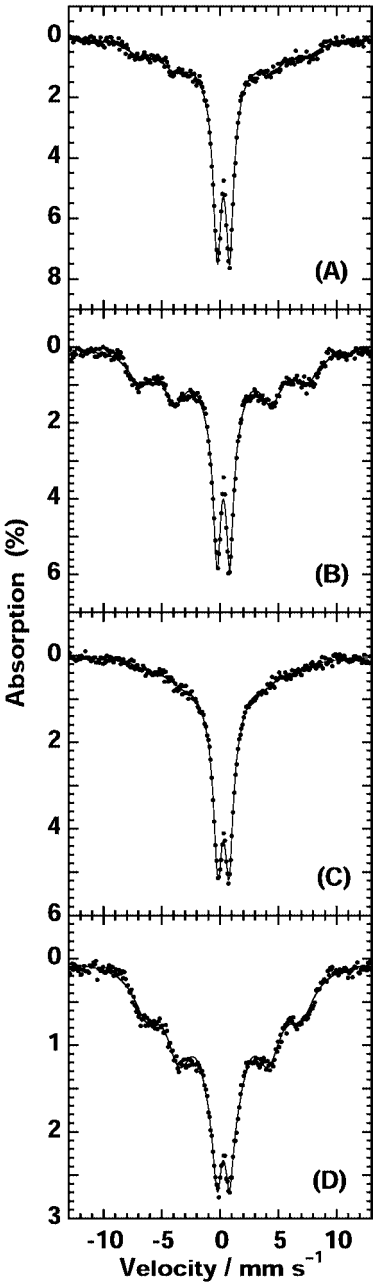

Fig. 6 Mössbauer spectra of the X_1-T4 sample at 84 K (A) and 77 K (B) and of the A_1-T4 sample at 90 K (C) and 77 K (D). The experimental points (dots) and the calculated data (solid line) are shown.

factor. The recoil-free factor of the iron changes for atoms with different oxidation numbers and in different local environments; in this case, the two components correspond to atoms which differ only for the state of the particle. Therefore the ratio of the areas can be considered equal to the ratio of the number of atoms.[21] The results of the fitting procedure are reported in Table 1.

These spectra show the evolution of the sample from the superparamagnetic state to the blocked state. The Mössbauer blocking temperature (T_{BM}) is defined by the condition that the area of the blocked component equals the area of the superparamagnetic component.[15] The T_{BM} for the X_1-T4 sample, which has been calculated by a linear extrapolation of the relative areas in the spectra at 77 K and 84 K, was found to be 88 ± 6 K.

The hyperfine magnetic field of the X_1-T4 sample at 4.2 K is 50.2 T, as reported elsewhere,[22] which is a typical value of nanocrystalline maghemite.[15]

In Fig. 6 the spectra of the A_1-T4 sample at temperatures of 90 K and 77 K are also shown; the results of the fits are given in Table 1. This sample presents a Zeeman splitted component in the spectrum at 90 K; at 77 K this component largely prevails. The T_{BM}, determined by using the areas of the components at 77 K and 90 K with a linear extrapolation, was found to be 93 ± 6 K.

The broadening of the lines of the Zeeman split components is an effect of the size distribution of the particles; particles with different volume have a magnetic reduced magnetic field because of the effect of the collective magnetic excitations.[23,24] The FWHM of the Zeeman split component is larger in the A_1-T4 than in the X_1-T4 sample at 77 K indicating a broader size distribution in the A_1-T4 sample.

Magnetic measurements

The temperature dependences of the ZFC and FC magnetizations of the X_1-T4, A_1-T4, A_2-T4 and A_2P-T4 samples are shown in Fig. 7. In all samples the two curves coincide at high temperature and the susceptibility follows, to a first approximation, a Curie–Weiss law. On decreasing temperature they begin to separate and the ZFC magnetization exhibits a narrow maximum. Such behaviour is characteristic of superparamagnetism[25] and is due to the progressive deblocking of particles of increasing size as temperature increases.

It is generally assumed that the temperature of the ZFC maximum, T_{max}, is directly proportional to the average blocking temperature, $T_{max} = \beta T_B$, where β is a constant depending on the shape of the size distribution.[26,27] The temperature at which the ZFC and FC curves begin to separate (T_{sep}) corresponds to the blocking of the largest particles. The difference $T_{sep} - T_{max}$ is therefore a qualitative measure of the width of the energy barrier distribution and thus of the nanoparticle size distribution.

The ZFC curve of the X_1-T4 sample has a maximum at 93 K and separates from the FC curve at about 120 K. The A_1-T4 sample displays a smaller T_{max} (72 K) but has a larger T_{sep} (larger than 200 K) which indicates a broader distribution of the effective energy barriers. These results are in good agreement with the size distribution obtained by TEM which indicated a smaller average size and a broader size distribution for the A_1-T4 sample.

The ZFC curves of the A_2-T4 and A_2P-T4 samples both peak around 60 K and separate from the FC curves near 150 K. In contrast to what was observed for the two samples discussed above the FC, magnetization sharply increases on lowering the temperature below T_{max}.

The field dependence of the magnetization in the range ± 6 Oe was measured at different temperatures for the four samples. The hysteresis loops measured at 3 K for the X_1-T4 and A_1-T4 sample are shown in Fig. 8(A) and (B), respectively. Both curves display the typical features of randomly oriented assemblies of nanosize single domain particles: the loops are open up to about 5 T and the coercivities are much larger than the bulk value and very large for an iron oxide based nanocomposite, being 1260 Oe and 1680 Oe for the X_1-T4 and A_1-T4 samples, respectively. In both samples the magnetization is far from saturation even at the highest measuring field and the saturation values extrapolated from the high field part of the curves (42 and 37 emu g^{-1} for the X_1-T4 and A_1-T4 samples) are much lower than that of bulk maghemite (82 emu g^{-1}).[28] The reduced remanence values are 0.15 for the A_1-T4 sample and 0.13 for the X_1-T4 one. These values are much lower than 0.5, as expected for randomly oriented, blocked nanoparticles. The discrepancy can be ascribed to the occurrence of a non-negligible fraction of small particles which are still relaxing fast at 3 K or to a small fraction of free paramagnetic Fe^{3+} ions. This is indeed confirmed by the low

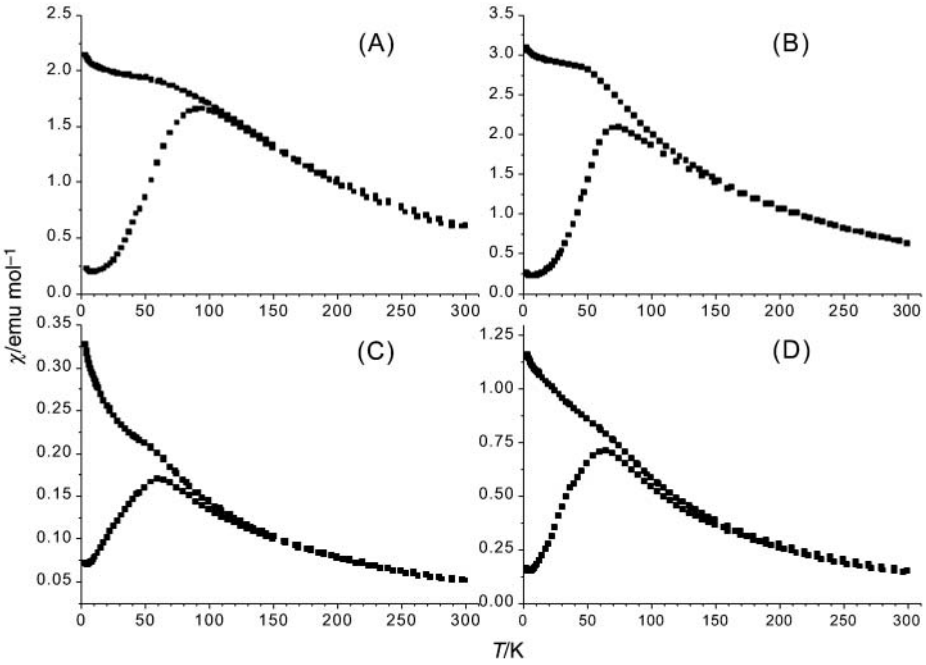

Fig. 7 ZFC and FC magnetizations of X_1-T4 (A), A_1-T4 (B), A_2-T4 (C) and A_2P-T4 (D). All the curves were measured with an applied field of 50 Oe.

temperature paramagnetic tails observed in both the ZFC and the FC magnetizations of the two samples.

The appearance of the hysteresis loops of samples A_2-T4 and A_2P-T4 is essentially the same as those shown in Fig. 8. Coercive fields are 0.179 and 0.188 T for A_2-T4 and A_2P-T4, respectively. Saturation magnetizations are smaller than those observed in the other two samples ($M_S = 24.8$ emu g^{-1} for A_2-T4 and 20.1 emu g^{-1} for A_2P-T4) as a result of the smaller average sizes and the presence of a small amount of the antiferromagnetic phase α-Fe_2O_3 whose contribution to M_S is much lower than that of maghemite. In Fig. 9 and 10 the coercive fields, H_C, and reduced remanences, M_R/M_{6T}, of samples X_1-T4 and A_1-T4 as a function of temperature are shown. At temperatures higher than those reported on the

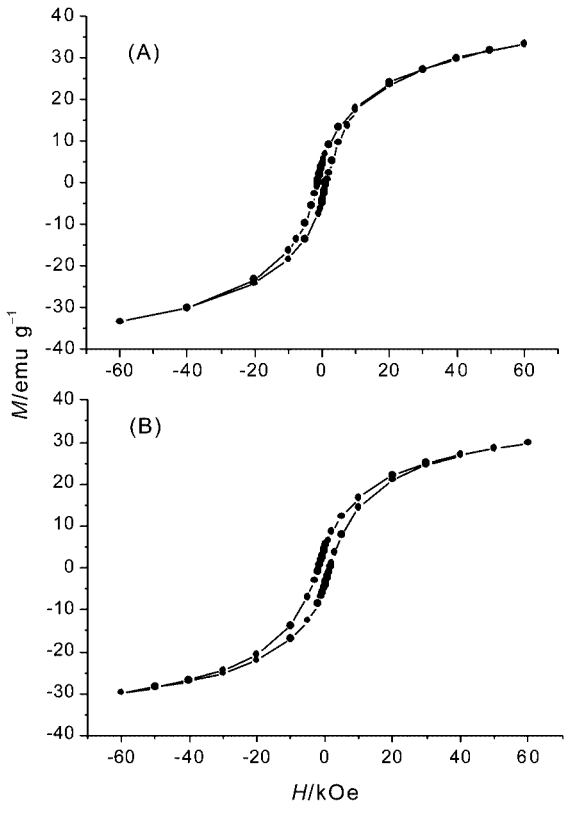

Fig. 8 Hysteresis loops of the X_1-T4 (A) and A_1-T4 (B) samples measured at 3 K.

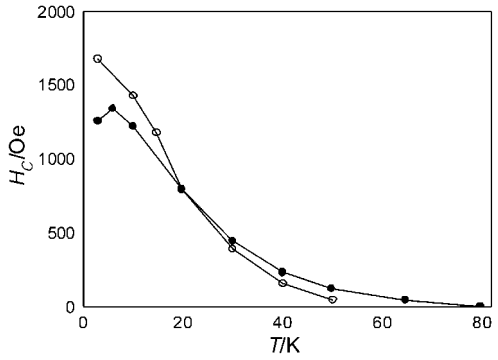

Fig. 9 Temperature dependence of the coercive field of X1-T4 (●) and A_1-T4 (○). The $T^{0.77}$ law predicted by the Stoner–Wohlfarth model is not obeyed by the two samples. The lines are a guide to the eyes.

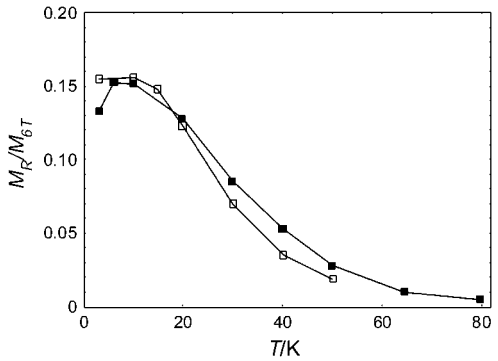

Fig. 10 Reduced remanence as a function of temperature measured from hysteresis loops for the X_1-T4 sample (■) and the A_1-T4 one (□). The lines are a guide to the eyes.

graphs H_C becomes negligible for both samples and the magnetization curves appear reversible. An anomalous increase of both H_C and M_R/M_{6T} when the temperature is increased from 3 to 6 K is observed for the X_1-T4 sample. Furthermore, neither for the X_1-T4 sample nor for the A_1-T4 sample do the expected decreases of H_C and M_R/M_{6T} with temperature obey the law predicted by the Stoner–Wolfarth model for an assembly of non-interacting single domain particles with a random distribution of easy axes $H_C = H_C(0)(1-(T/T_B)^{0.77})$ where $H_C(0)$ is the coercivity at 0 K which for uniaxial anisotropy is equal to $0.96\,K/M_S$, K being the effective anisotropy constant and M_S the saturation magnetization.[29] The large deviations from the law, as well as the anomalous H_C maximum, can be reasonably ascribed to interparticle interactions.

In fact, TEM micrographs revealed the presence of several large aggregates including a large number of particles in close contact with each other. Interparticle interactions are therefore expected to be relevant in both A_1-T4 and X_1-T4 samples and then to influence the process of reorientation of the magnetization. These interactions are expected to be mainly dipole–dipole but, due to the close contact between particles, exchange interactions between surface atoms belonging to neighboring particles cannot be ruled out. If interparticle interactions are not too strong, their effects can be described as a modification of the energy barrier of each particle and the dynamical properties can still be interpreted within the Néel–Brown model for superparamagnetism.[30,31] On the other hand, in the case of strong interactions, the strong correlation between magnetic moments does not allow one to define the energy barrier for a single particle and a drastic change of regime, where the relaxation process is the result of collective dynamics, can occur. Due to the random distribution of the magnetic moments and to the frustration of magnetic interactions, it has been suggested that the freezing of such a system can result in a low temperature collective state which resembles the spin-glass phase.[32] Evidence of spin-glass like behavior has been indeed reported for several different nanosized materials.[15,33–35] However, the onset of this collective spin-glass like state (*i.e.* whether the freezing is really a phase transition from a superparamagnetic to a spin-glass like state or not) is still matter of debate.[30,36–38]

The different mechanisms of relaxation of the magnetization can be distinguished by a.c. susceptibility experiments. In Fig. 11 the temperature dependence of the in-phase component, χ', of the A_1-T4 (Fig. 11(A)) and X_1-T4 (Fig. 11(B)) samples, measured at different frequencies in the range 0.18–510 Hz, is shown. At high temperature, χ' is frequency independent and follows approximately a Curie–Weiss law. On decreasing temperature it deviates from this law and a maximum appears. At the same time the imaginary part of the a.c. susceptibility, χ'', departs from zero showing a peak corresponding to the inflection point of χ'. The positions of the maxima of both the real and imaginary components are frequency dependent, moving to lower temperatures as frequency decreases. The average relaxation time τ can be extracted from χ' curves assuming that $\tau = 1/\nu$ at the temperature of the maximum.

In the inset of Fig. 11 $\ln(\tau)$ is plotted as a function of $(1/T_{Max})$. For both samples a linearity is observed as predicted by the Néel–Brown model for superparamagnetism.[23,25] In fact, according to the model the relaxation time should follow an Arrhenius law $\tau = \tau_0 \exp(\Delta/k_B T)$ where Δ is the energy barrier which is given by $\Delta = KV$, V being the average particle volume, k_B the Boltzmann constant and τ_0 a time constant of the order of 10^{-9}–10^{-12} s. However, the linear fits of the data give unrealistically large values for the energy barriers and unphysical pre-exponential factors (smaller than 10^{-25}). The inadequacy of the Arrhenius law indicates that the relaxation process is not governed by the simple blocking of each magnetic moment but is rather strongly influenced by a cooperative mechanism related to the presence of interparticle interactions.

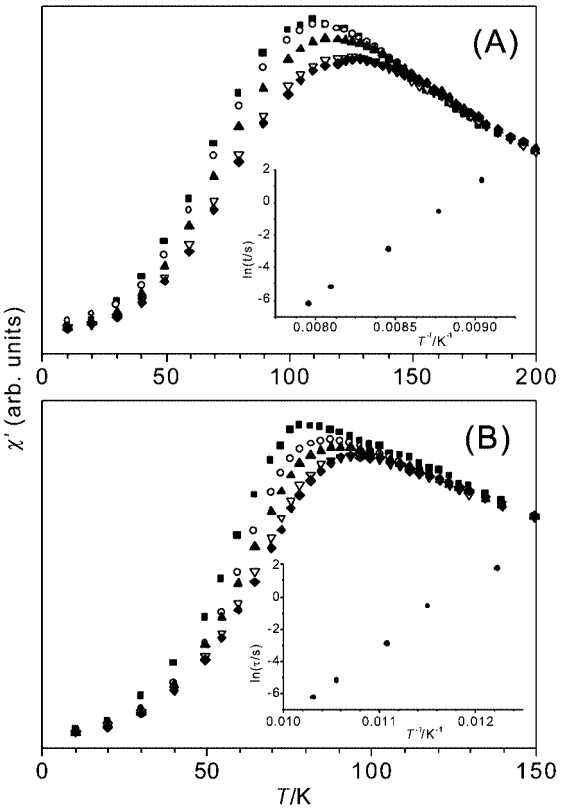

Fig. 11 Temperature dependence of the real part χ' of the a.c. susceptibility measured at different frequencies in the range 0.18–510 Hz for X_1-T4 (A) and A_1-T4 (B). In the inset the $\ln\tau$ *vs.* $1/T_{max}$ plots are shown.

The frequency dependence of the χ' maximum cannot be satisfactorily reproduced even by the dynamic scaling laws proposed for spin glasses, the Vogel–Fulcher law and the power law, $\tau = \tau_0[T_g/(T-T_g)]^{-z\nu}$. The Vogel–Fulcher law is a modified Arrhenius law where T is replaced by $T-T_0$, where T_0 is a measure of the interparticle interactions. It was originally introduced for spin glasses[39] and later proposed for magnetically interacting particles at $T \gg T_0$.[40] On the other hand, a critical slowing down of the relaxation according to a power law is characteristic of spin glasses with a true thermodynamic transition at $T = T_g$.

A criterion which can be used to analyze the frequency dependence of χ' for spin glasses and other slow relaxing magnetic systems is based on the relative variation of T_{max} per frequency decade, $\Delta T_{max}/(T_{max}\Delta\log\nu)$.[41] In our case we obtained about 0.04 for both samples. The value is in between those reported for systems that show a thermodynamic transition to a spin-glass phase and superparamagnetic systems and it is near to those observed in systems for which evidence of progressive inhomogeneous freezing was reported.[42]

Conclusions

This sol–gel procedure was successful for obtaining pure maghemite–silica nanocomposites starting from both xerogel and aerogel samples, with average particle size around 5 nm. This is a remarkable result in comparison with previous investigations where maghemite was always accompanied by hematite in aerogel Fe_2O_3–SiO_2 materials[12] and also in the corresponding xerogel samples hematite was easily formed for iron contents higher than 23%.[11] However, particular care has

to be taken when preparing aerogel samples because the pure γ-Fe_2O_3–SiO_2 nanocomposite is obtained only when starting from a gel which contains a small amount of solvent entrapped in the pores.

It should be pointed out that previous results were obtained using a different sol–gel procedure and different conditions of heat treatment. In particular, in the previous investigations maghemite precursors were shown to be either 2-line (XRD) ferrihydrite for the xerogel samples or 6-line ferrihydrite for the aerogel ones. In the present case, in accordance with ref. 13, the mechanism of formation of maghemite involves first the formation of Fe_3O_4 *via* the reduction of the Fe(III) ions by the organics present in the gels, followed by the oxidation of Fe_3O_4 to γ-Fe_2O_3.

In the xerogel samples, which are directly formed from the gels, the organics mainly come from the solvent entrapped in the pores at the gelation point. In this case the average size of the maghemite nanoparticles is higher for the sample prepared starting from a gel entrapping a larger amount of solvent. On the other hand, in the aerogels the solvent is removed by high temperature supercritical drying; at the same time, the esterification of the silanol groups from the ethanol present in the autoclave produces a large amount of new organic residues which are responsible for magnetite and maghemite formation. The combustion of the organics in the aerogel samples gives rise to strongly exothermic peaks due to the high surface area and high reactivity of this kind of material. In particular, if the combustion of the organics gives rise to local overheating of the sample, a maghemite to hematite transition may occur. This interpretation is confirmed by the absence of hematite impurities in the A_2P-T4 sample because the reaction is less strong in the powdered sample.

The ratio of the Mössbauer blocking temperature and the T_{max} of the ZFC susceptibility, for the X_1-T4 and A_1-T4 samples, is much smaller than that predicted following the Neèl theory for non-interacting particles (ratio in the range 2–7)[15] pointing out the presence of strong interactions between nanoparticles. These results are in agreement with TEM observations, which showed the formation of nanoparticle agglomerates. Accordingly, the magnetic data of the X_1-T4 and A_1-T4 samples indicate that their magnetic properties are strongly influenced by interparticle interactions. The observed frequency dependence of T_{max} cannot be described either by single particle blocking or by a phase transition from a superparamagnetic state to a spin-glass like ordered state. Due to the occurrence of an energy barrier distribution and to the simultaneous presence of isolated and agglomerated particles, single particle effects and collective freezing of particle moments will coexist, resulting in more complex behavior which appears as an inhomogeneous freezing with no phase transition.

Acknowledgements

The authors would like to thank CNR and MURST for financial support and Cesar de Julian Fernandez for useful discussion.

References

1 C. Chanéac, E. Tronc and J. P. Jolivet, *Nanostruct. Mater.*, 1995, **6**, 715.
2 R. F. Ziolo, E. P. Giannelis, B. A. Weinstein, M. P. O'Horo, B. N. Ganguly, V. Mehrotra, M. W. Russel and D. R. Huffman, *Science*, 1992, **257**, 219.
3 C. R. F. Lund and J. A. Dumesic, *J. Phys. Chem.*, 1981, **85**, 3075.
4 R. E. Newnham, S. E. McKinstry and H. Ikaua, *Mater. Res. Soc. Symp. Proc.*, 1990, **175**, 161.
5 D. Vollath, D. V. Szabo, R. D. Taylor, J. O. Willis and K. E. Sickafus, *Nanostruct. Mater.*, 1995, **6**, 941.
6 K. Haneda and A. H. Morrish, *Solid State Commun.*, 1977, **22**, 779.
7 M. P. Morales, C. Pecharroman, T. Gonzales Carreno and C. J. Serna, *J. Solid State Chem.*, 1994, **108**, 158.
8 G. Ennas, G. Marongiu, A. Musinu, A. Falqui, P. Ballirano and R. Caminiti, *J. Mater. Res.*, 1999, **14**, 1570.
9 G. Piccaluga, A. Corrias, G. Ennas and A. Musinu, *Mater. Res. Found.*, 2000, **13**, 1.
10 C. J. Brinker and G. W. Scherer, *Sol–Gel Science*, Academic Press, San Diego, 1990.
11 C. Cannas, D. Gatteschi, A. Musinu, G. Piccaluga and C. Sangregorio, *J. Phys. Chem. B*, 1998, **102**, 7721.
12 M. F. Casula, A. Corrias and G. Paschina, *J. Non-Cryst. Solids*, 2001, **293–295**, 25.
13 F. del Monte, M. P. Morales, D. Levy, A. Fernandez, M. Ocana, A. Roig, E. Molins, K. O'Grady and C. J. Serna, *Langmuir*, 1997, **13**, 3627.
14 H. H. Wickman, *Mössbauer Effect Methodology*, ed. I. J. Gruverman, Plenum Press, New York, 1966, vol. 2, p. 39.
15 S. Mørup, F. Bødker, P. V. Hendriksen and S. Linderoth, *Phys. Rev. B*, 1995, **52**, 287.
16 E. Tronc, P. Prene, J. P. Jolivet, F. d'Orazio, F. Lucari, D. Fiorani, M. Godinho, R. Cherkaoui, M. Nogues and J. L. Dorman, *Hyperfine Interact.*, 1995, **95**, 129.
17 M. Prassas, J. Phalippou and J. Zarzycki, *J. Mater. Sci.*, 1984, **19**, 1656.
18 M. F. Casula, A. Corrias and G. Paschina, *J. Mater. Res.*, 2000, **15**, 2187.
19 PDF-2 File, JCPDS International Centre for Diffraction Data, 1601 Park Lane, Swarthmore, PA, USA.
20 P. Gutlich, R. Link and A. Trautwein, *Mössbauer Spectroscopy and Transition Metal Chemistry*, Springer Verlag, Berlin, 1978, vol. 56.
21 M. Dyar, *Am. Mineral.*, 1985, **70**, 304.
22 C. Cannas, G. Concas, F. Congiu, A. Musinu, G. Piccaluga and G. Spano, *J. Phys. Chem. Solids,* submitted.
23 W. F. Jr. Brown, *Phys. Rev.*, 1963, **130**, 1677.
24 S. Mørup, H. Topsoe and J. Lipka, *J. Phys. C*, 1976, **35**, 207.
25 L. Néel, *Ann. Geophys.*, 1949, **5**, 99.
26 J. I. Gittlemann, B. Abeles and S. Bozowski, *Phys. Rev. B*, 1974, **9**, 3891.
27 M. El-Hilo, K. O'Grady and R. W. Chantrell, *J. Magn. Magn. Mater.*, 1992, **117**, 21.
28 R. M. Cornell and U. Schwertmann, in *The Iron Oxides, Structure, Properties, Reaction, Occurrence and Uses*, VCH Verlagsgesellschaft, Weinheim and New York, 1996.
29 E. C. Stoner and E. P. Wohlfarth, *Philos. Trans. R. Soc. London A*, 1948, **240**, 599.
30 J. L. Dormann, L. Bessais and D. Fiorani, *J. Phys. C: Solid State Phys.*, 1988, **21**, 2015.
31 J. L. Dormann, F. D'Orazio, F. Lucari, E. Tronc, P. Prene, J. P. Jolivet, D. Fiorani, R. Chekaoui and M. Nogues, *Phys. Rev. B*, 1996, **53**, 12291.
32 W. Luo, S. R. Nagel, T. F. Rosenbaum and R. E. Rosenzweig, *Phys. Rev. Lett.*, 1991, **67**, 2121.
33 J. L. Dormann, R. Chekaoui, L. Spinu, M. Nogues, F Lucari, F. D'Orazio, D. Fiorani, A. Garcia, E. Tronc and J. P. Jolivet, *J. Magn. Magn. Mater.*, 1998, **187**, L139.
34 C. Djurberg, P. Svedlindh, P. Nordblad, M. F. Hansen, F. Bødker and S. Mørup, *Phys. Rev. Lett.*, 1997, **79**, 5154.
35 T. Jonsson, P. Nordlab and P. Svedlinh, *Phys. Rev. B*, 1998, **57**, 497.
36 D. Fiorani, J. L. Dormann, R. Chekaoui, E. Tronc, F. Lucari, F. D'Orazio, L. Spinu, M. Nogues, A. Garcia and A. M. Testa, *J. Magn. Magn. Mater.*, 1999, **196–197**, 143.
37 M. García del Muro, X. Battle and A. Labarta, *J. Magn. Magn. Mater.*, 2000, **221**, 26.
38 M. F. Hansen and S. Mørup, *J. Magn. Magn. Mater.*, 1998, **184**, 262.
39 J. L. Tholence, *Solid State Commun.*, 1980, **35**, 113.
40 S. Shtrikman and E. P. Wohlfart, *Phys. Lett. A*, 1981, **85**, 467.
41 J. A. Mydosh, *Spin Glasses: an Experimental Introduction*, Taylor & Francis Ltd., London, 1993.
42 J. L. Dormann, D. Fiorani, E. Tronc, in *Advances in Chemical Physics*, ed. I. Prigogine and S. A. Rice, Wiley & Sons, New York, 1997, vol. 98, p. 283.